Supplementary Article

NiCr-LDH/V_4C_3 MXene Nanocomposites as an Efficient Electrocatalyst for Urea Oxidation.

Dana Susan Abraham,[a] Mari Vinoba,[b] and Margandan Bhagiyalakshmi [a*]

[a] *Department of Chemistry, Central University of Kerala, India*

[b] *Kuwait Institute for Scientific Research, Safat-13109, Kuwait*

Materials Characterization

Surface morphologies of the synthesized NCV-21 nanocomposites were analyzed using FE-SEM (SUPRA 55 VP- 4132 CARL ZEISS) with an attached Energy Dispersive Spectrometer (EDS), and transmission electron microscopy (TEM, Tecnai™ G2 20). The Zeta potential measurement was carried out on the Horiba-SZ 100 model Zeta potential analyzer at pH = 7. The crystal structure analysis was carried out using a PANalytical (Empyrean) X-ray diffractometer (Cu Kα radiation - 0.154 nm) in the range of 5 to 90° with a step size of 0.02° s^{-1}. The presence of functional groups in NCV nanocomposites was verified by FTIR spectroscopy (Perkin Elmer infrared spectrometer), using the ATR technique in the range of 400-4000 cm^{-1}. The textural properties were analyzed using Quantachrome Instruments (Nova Touch lx4 Model) BET Surface area analyzer. The X-ray photoelectron spectra (XPS) for the sample were captured using a Thermo Scientific instrument (Model: K-Alpha-KAN9954133). Electrochemical characteristics were analyzed using a Bio-Logic (SP-240) electrochemical workstation.

Scheme

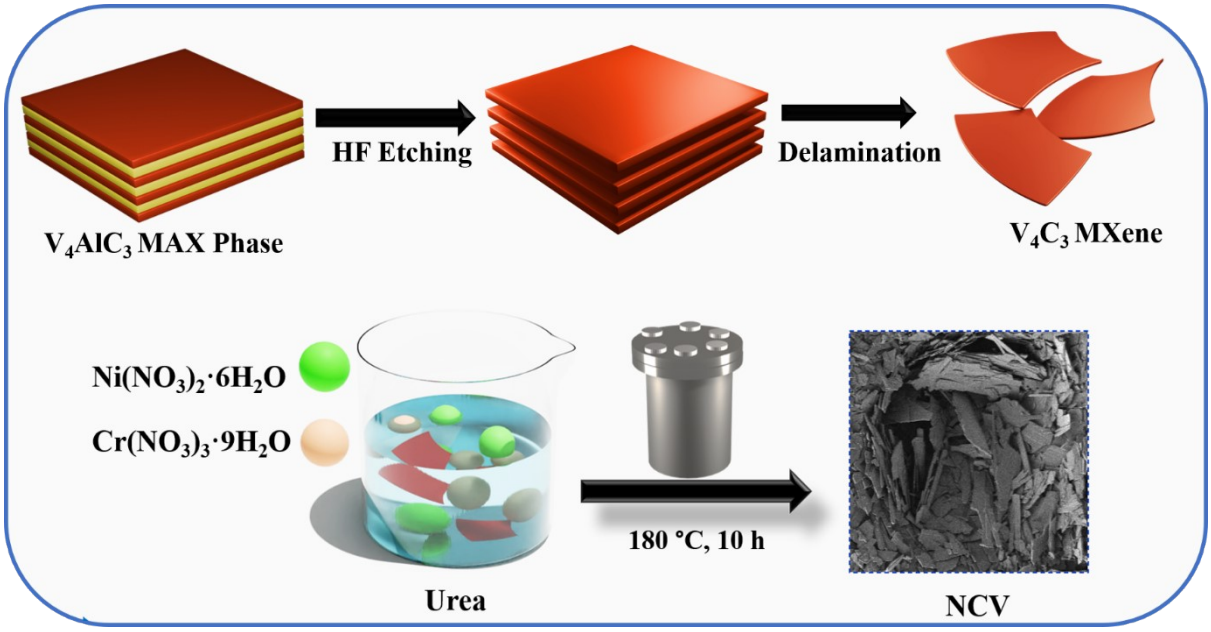

Fig. S1 Schematic representation of NiCr-LDH/V_4C_3 MXene (NCV) synthesis.

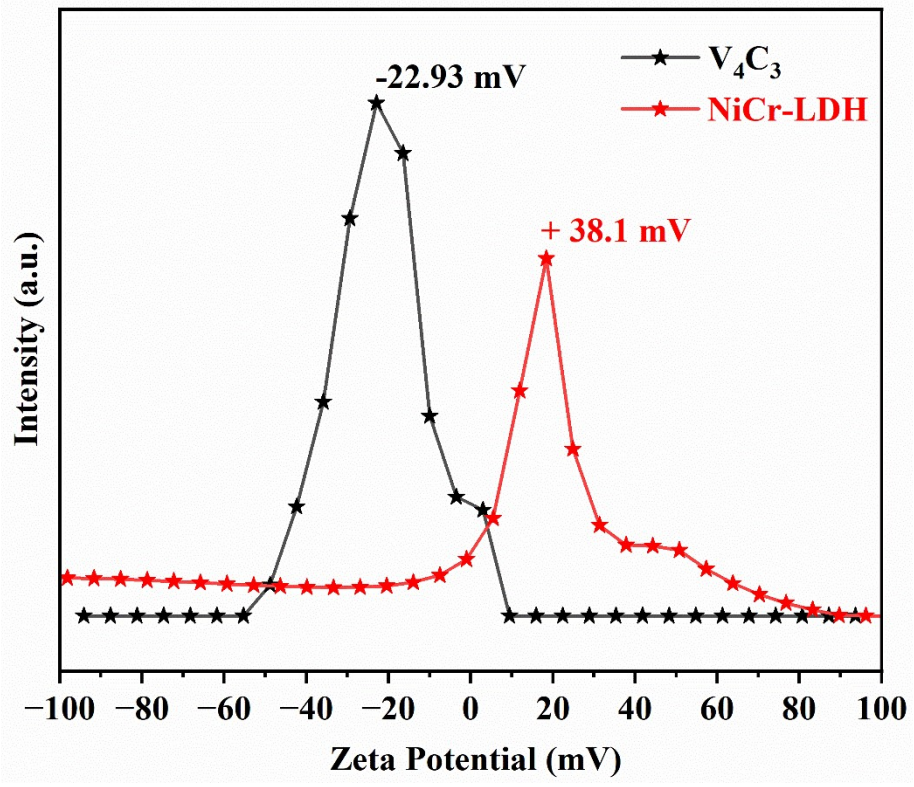

Fig. S2 Zeta potential of V_4C_3 and NiCr-LDH.

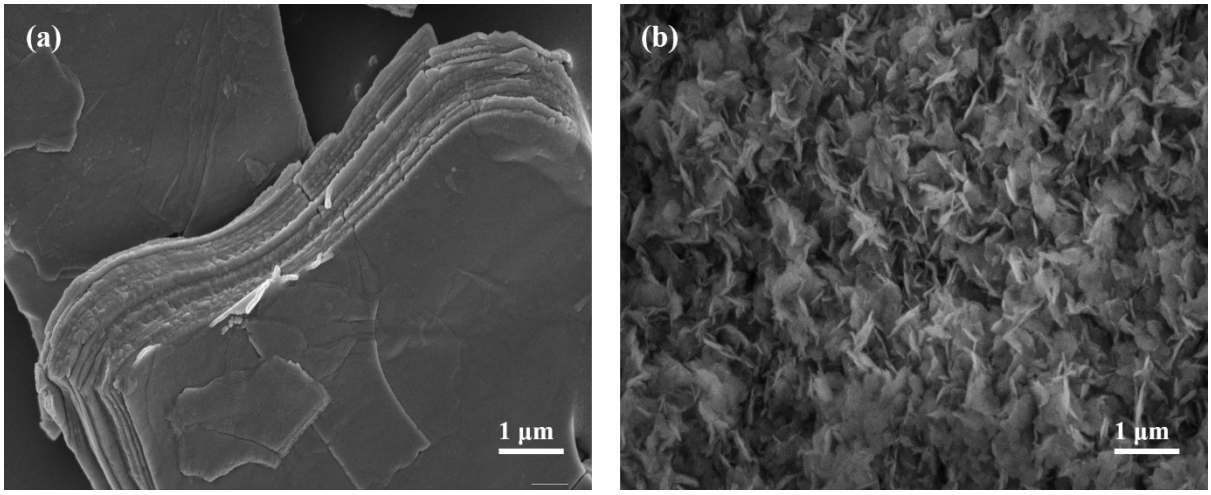

Fig. S3 (a) FE-SEM image of V_4C_3 MXene, and (b) NiCr-LDH.

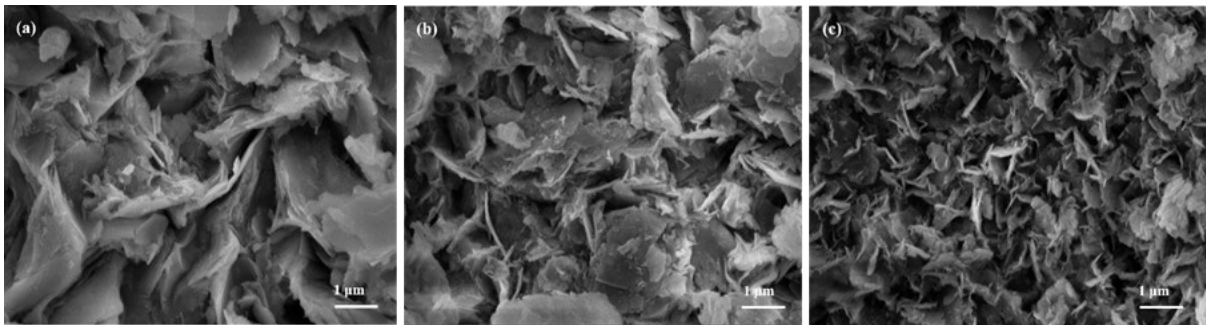

Fig. S4 FE-SEM image of NCV nanocomposites (a) NCV-11, (b) NCV-12, and (c) NCV-31.

It is evident from the FE-SEM images of all the NCV nanocomposites that a nanoflake-like architecture is formed. The NCV-21 nanocomposite exhibited nanostructured nanosheet-like morphologies,[1] indicating that the 2D layered NiCr-LDH and V_4C_3 MXene underwent exfoliation during synthesis, forming thin nanosheets. The structural composition, characterized by thin nanosheet, could promote the diffusion of electrolyte ions into internal active sites,[2] thereby facilitating the kinetics of the urea oxidation reaction. Meanwhile, NCV-11, NCV-12, and NCV-31 exhibited curved nanoflake-like structures, which are different from the NCV-21 structure, which might be due to incomplete composite formation. Further, Cr content in NiCr-LDH also affects the crystallinity of the nanocomposite, as evident from the XRD analysis, which is also consistent with previous reports.[3]

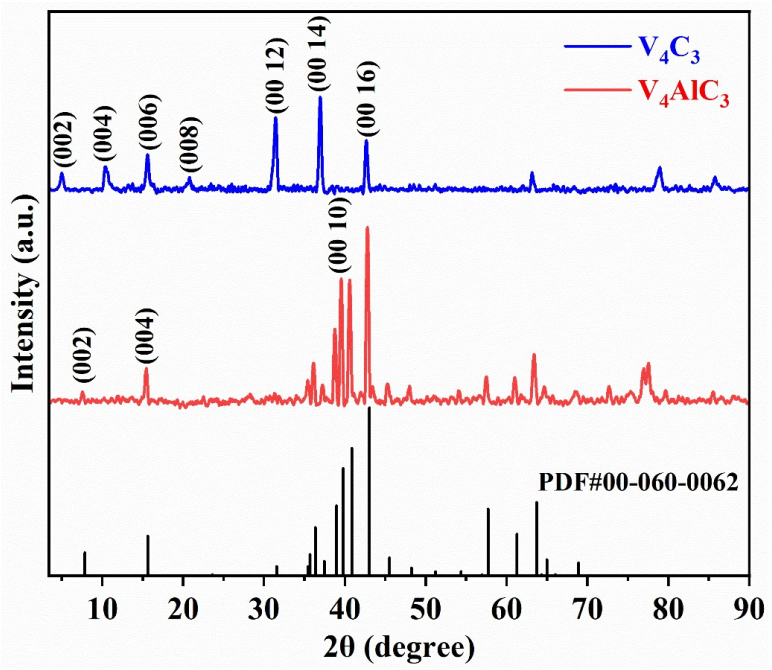

Fig. S5 XRD Pattern of V_4AlC_3 MAX and V_4C_3 MXene.

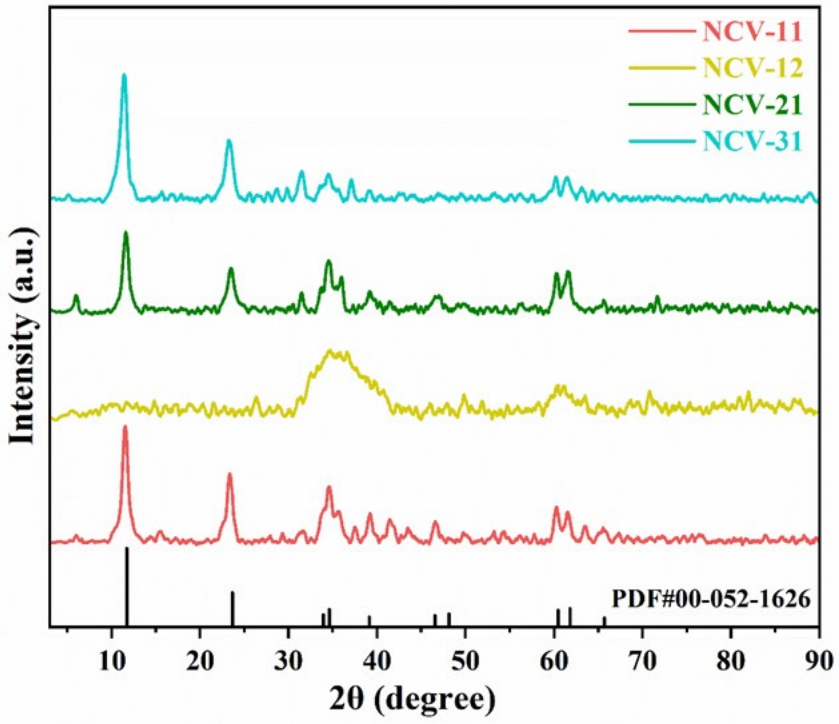

Fig. S6 XRD pattern of NCV nanocomposites.

Fig. S6 depicts the XRD pattern of other NCV nanocomposites. The distinctive XRD peaks of V_4C_3 MXene and NiCr-LDH are shown in the NCV-11, NCV-21, and NCV-31, while NCV-12 lacks the characteristics peaks of V_4C_3 MXene and NiCr-LDH. Moreover, the

presence of the characteristic (002) plane of V_4C_3 MXene after compositing with NiCr-LDH in NCV-11, NCV-21, and NCV-31 confirms the successful formation of the NiCr-LDH/V_4C_3 MXene nanocomposite.[4] An increase in Cr concentration in NCV-12 resulted in a decrease in crystalline peak intensity, indicating that Cr disrupted the crystalline structure of Ni and led to a more amorphous nature, aligning with earlier reports.[5] Further, NCV-21 exhibited sharp XRD peaks due to V_4C_3 MXene and NiCr-LDH, which contributed to the synergistic effect between V_4C_3 MXene and NiCr-LDH in NCV-21 that resulted in enhanced UOR activity. The structural composition of NCV-21, characterized by thin nanosheets and high crystallinity, promotes the diffusion of electrolyte ions into internal active sites,[2] thereby facilitating the kinetics of the urea oxidation reaction compared to other compositions.

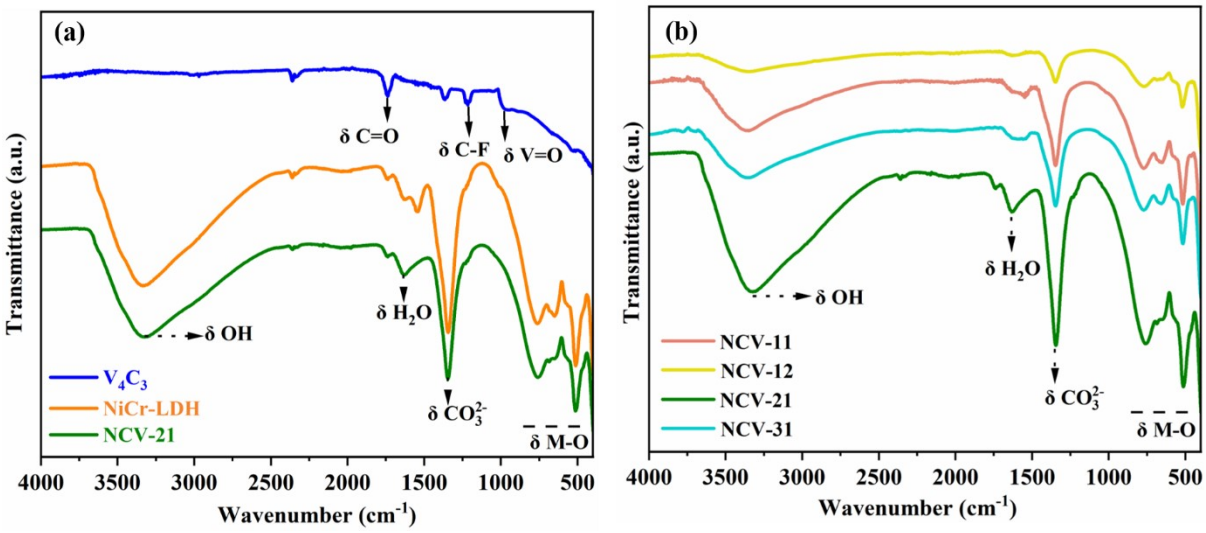

Fig. S7 FT-IR spectrum of V_4C_3 MXene, NiCr-LDH, and NCV-21 nanocomposite, (b) NCV-11, NCV-12, NCV-21 and NCV-31 nanocomposites.

Fig. S7a shows the FT-IR analysis of pristine V_4C_3 MXene, NiCr-LDH, and NCV-21. The characteristic peaks at 1739, 1212, and 989 cm^{-1} correspond to the C=O,[6] C-F,[7] and V=O[8] bands of V_4C_3 MXene. The NiCr-LDH presents the characteristic peak of LDH at 3340 cm^{-1}, which is attributed to the OH group of interlayer water molecules in the LDH structure and the OH stretching of metal hydroxyls.[9] The absorption band at 1630 cm^{-1} arises from the bending vibration of H_2O molecules in the interlayer spacing.[10] Also, the band at 1347 cm^{-1} is assigned to the vibrational mode of CO_3^{2-} ions in the interlayers of NiCr-LDH.[11] Furthermore, the peaks below 1000 cm^{-1} are attributed to M–O, O–M–O, and M–O–M bonds.[12] NCV-21 nanocomposites predominantly show the characteristic peaks of NiCr-LDH due to the

minimum amount of V_4C_3 MXene in the nanocomposite. Further, the characteristic peaks of MXene would have overlapped by the NiCr-LDH peaks.

Fig. S7b shows the FT-IR spectrum of the synthesized NCV-11, NCV-12, and NCV-31 nanocomposites. It can be observed that the NCV-11, NCV-12, and NCV-31 show the characteristic peak of NiCr-LDH; similar to NCV-21, the characteristic MXene peaks are overlapped by NiCr-LDH peaks.

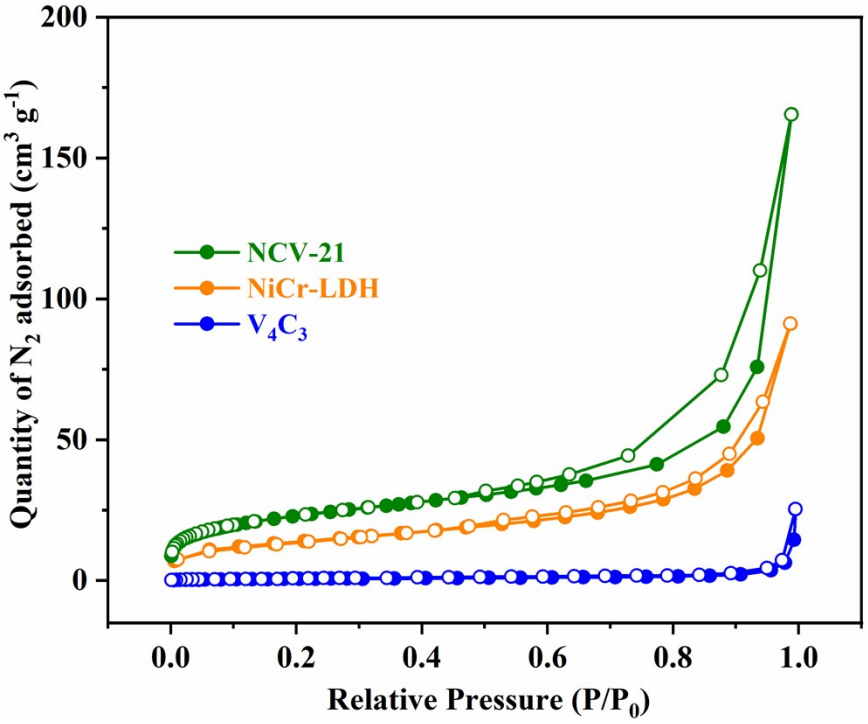

Fig. S8 (a) N_2 adsorption−desorption isotherm of V_4C_3, NiCr-LDH, and NCV-21.

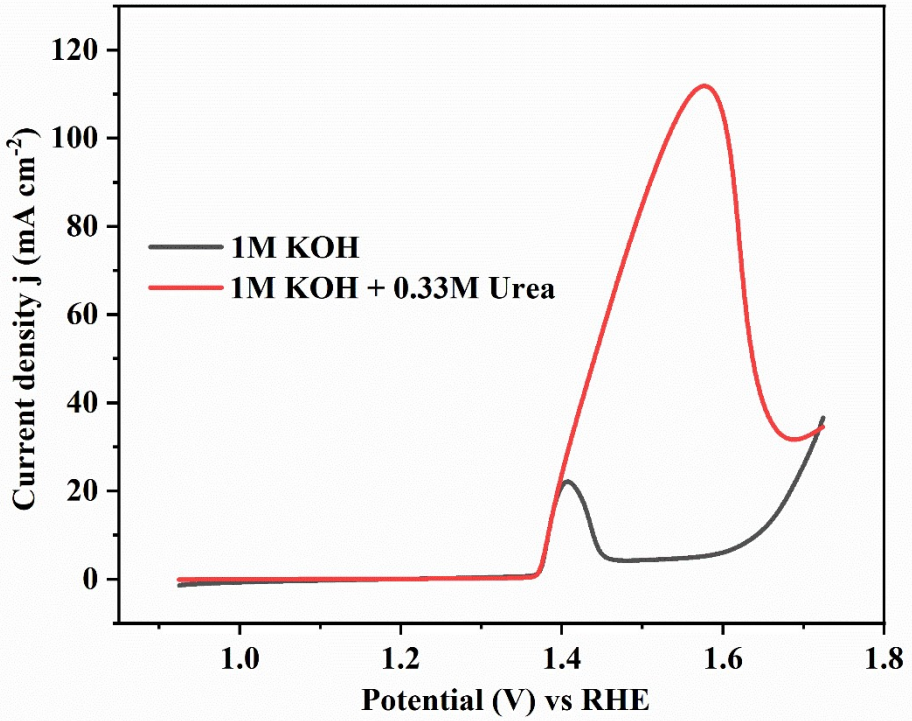

Fig. S9 LSV plot of NCV-21 in 1M KOH with and without 0.33 M Urea.

Raman Spectra of electrolyte after electro-oxidation of urea.

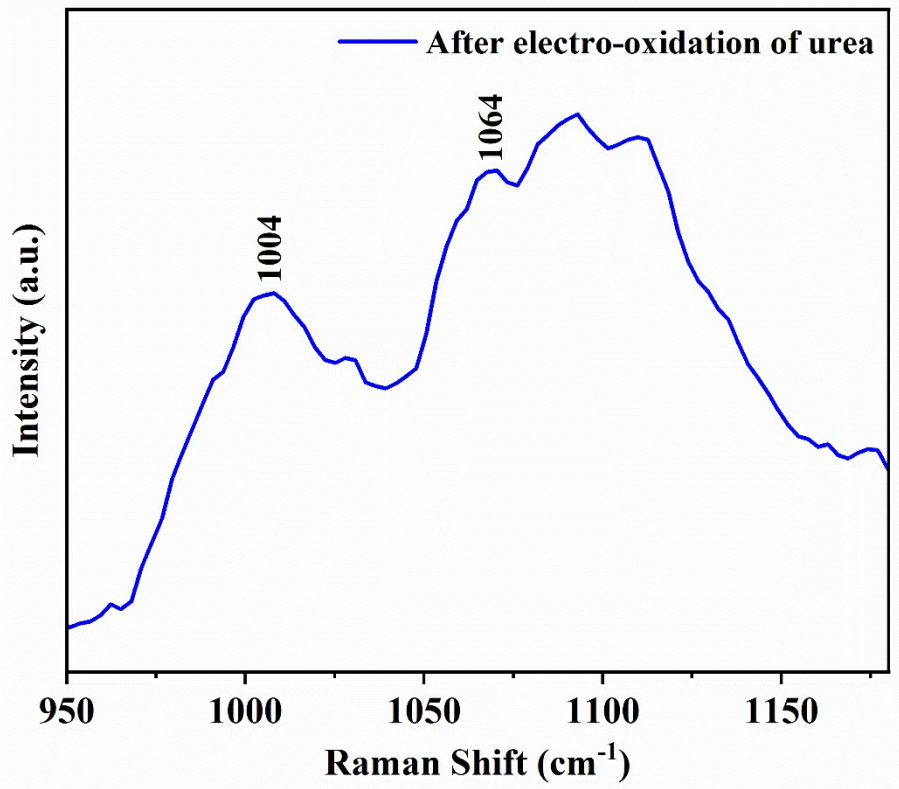

Fig. S10 Raman spectra of the electrolyte after electro-oxidation of urea by NCV-21 electrocatalyst.

References:

1. S. Biswal, B. Mishra, D. Pohl, B. Rellinghaus, D. Ghosh and B. P. Tripathi, *Journal of Materials Chemistry A*, 2024, **12**, 2491-2500.
2. Z. Chen, H. Deng, M. Zhang, Z. Yang, D. Hu, Y. Wang and K. Yan, *Nanoscale Advances*, 2020, **2**, 2099-2105.
3. X. Yan, W.-D. Zhang, H. Xu, L. Xiang, J. Liu, J. Yang, H. Zhu and Z.-G. Gu, *Electrochimica Acta*, 2021, **388**, 138633.
4. D. Zhang, J. Cao, X. Zhang, N. Insin, R. Liu and J. Qin, *ACS Applied Energy Materials*, 2020, **3**, 5949-5964.
5. K. Singh and A. Schechter, *ChemCatChem*, 2017, **9**, 3374-3379.
6. C. Zhou, Z. Li, S. Liu, L. Ma, T. Zhan and J. Wang, *Tribology Letters*, 2022, **70**, 63.
7. Z. U. D. Babar, J. Fatheema, N. Arif, M. Anwar, S. Gul, M. Iqbal and S. Rizwan, *RSC advances*, 2020, **10**, 25669-25678.
8. H. Chand, M. Sharma and V. Krishnan, *Separation and Purification Technology*, 2022, **292**, 121032.
9. N. S. Padalkar, S. V. Sadavar, R. B. Shinde, A. S. Patil, U. M. Patil, D. S. Dhawale, H. M. Pathan, S. D. Sartale, V. G. Parale and A. Vinu, *Advanced Materials Interfaces*, 2022, **9**, 2101216.
10. H. Sohrabi, M. R. Majidi, K. Asadpour-Zeynali, A. Khataee and A. Mokhtarzadeh, *Microchimica Acta*, 2023, **190**, 112.
11. S. Gamil, M. Antuch, I. Zedan, and W. M. El Rouby, *Colloids and Surfaces A: Physicochemical and Engineering Aspects*, 2020, **602**, 125067.
12. S. Gamil, W. M. El Rouby, M. Antuch and I. Zedan, *RSC advances*, 2019, **9**, 13503-13514.